.

Approaching the limits of two-phase boiling heat transfer: High heat flux and low superheat

J. W. Palko, C. Zhang, J. D. Wilbur, T. J. Dusseault, M. Asheghi, K. E. Goodson, and J. G. Santiago

Citation: Appl. Phys. Lett. **107**, 253903 (2015); doi: 10.1063/1.4938202
View online: http://dx.doi.org/10.1063/1.4938202
View Table of Contents: http://aip.scitation.org/toc/apl/107/25
Published by the American Institute of Physics

Articles you may be interested in

Suppressing high-frequency temperature oscillations in microchannels with surface structures
Appl. Phys. Lett. **110**, 033501033501 (2017); 10.1063/1.4974048

Hierarchically structured surfaces for boiling critical heat flux enhancement
Appl. Phys. Lett. **102**, 151602151602 (2013); 10.1063/1.4801811

Negative pressures in nanoporous membranes for thin film evaporation
Appl. Phys. Lett. **102**, 123103123103 (2013); 10.1063/1.4798243

Fearful for the future of science?
Sign up for FREE FYI emails.
AIP | American Institute of Physics

Approaching the limits of two-phase boiling heat transfer: High heat flux and low superheat

J. W. Palko,[a] C. Zhang, J. D. Wilbur, T. J. Dusseault, M. Asheghi, K. E. Goodson, and J. G. Santiago[a]
Department of Mechanical Engineering, Stanford University, Stanford, California 94305, USA

(Received 16 September 2015; accepted 1 December 2015; published online 23 December 2015)

We demonstrate capillary fed porous copper structures capable of dissipating over 1200 W cm^{-2} in boiling with water as the working fluid. Demonstrated superheats for this structure are dramatically lower than those previously reported at these high heat fluxes and are extremely insensitive to heat input. We show superheats of less than 10 K at maximum dissipation and varying less than 5 K over input heat flux ranges of 1000 W cm^{-2}. Fabrication of the porous copper layers using electrodeposition around a sacrificial template allows fine control of both microstructure and bulk geometry, producing structures less than 40 μm thick with active region lateral dimensions of 2 mm × 0.3 mm. The active region is volumetrically Joule heated by passing an electric current through the porous copper bulk material. We analyze the heat transfer performance of the structures and suggest a strong influence of pore size on superheat. We compare performance of the current structure to existing wick structures. © *2015 AIP Publishing LLC*.
[http://dx.doi.org/10.1063/1.4938202]

Porous structures are effective in enhancement of boiling and evaporation and play an important role in a large number of thermal management and energy conversion systems.[1–4] Often, these structures rely on capillary suction to deliver liquid to the phase change surface, and are ultimately limited by the competition between capillary driving force, which scales inversely with feature size, and the viscous resistance, which scales inversely with the square of feature size.[5] This competition, and the desire to operate at large wicking lengths, often limits the feature sizes that are applied in capillary fed porous structures for two-phase cooling.[2,6]

There have been a number of capillary fed structures demonstrated capable of dissipating large heat fluxes,[7–14] with some (e.g., Refs. 8 and 10) approaching or exceeding 1 kW cm^{-2}. However, the latter structures exhibit large superheat exceeding 75 K. Often these structures operate in a boiling regime. Systems may combine fine scale features for enhanced capillary suction and coarser features for liquid transport.[15,16] A variety of approaches have been applied to achieve the required microstructural control, including advanced particle processing techniques[8,13] and microfabrication.[10,12] Electrodeposition around a template presents a particularly interesting approach for controlling microstructure in highly thermally conductive materials. This method has been applied to form porous structures with extremely regular pore geometries for applications such as photonics.[17–19] Here, we apply an electrodeposition approach to generate finely porous copper structures for use in boiling heat transfer with similar or higher heat dissipation at substantially lower superheat than the best performing wicks to date in terms of heat dissipation, albeit with short liquid transport lengths.

In this letter, we demonstrate heat dissipation exceeding 1200 W cm^{-2} by boiling water from volumetrically Joule heated porous copper structures using a passive capillary feed. Of particular interest, superheats displayed by this system are low (<10 K at 1200 W cm^{-2}) and remarkably insensitive to heat flux (varying by <5 K over 1000 W cm^{-2}). We apply templated electrodeposition to define these thin (<40 μm) porous structures, which have finely controlled microstructure including small, uniform pores (5 μm), over 2 mm × 0.3 mm active areas.

Fig. 1 shows a schematic (a) of the experimental configuration and the geometry of the porous copper sample used (b). The active region is volumetrically self-heated by passing a current through it, and its temperature is determined from the calibrated resistance of the porous copper. The electrical measurement setup is described fully in the supplementary material document.[20] A high permeability cellulose wick supplies the active region with room temperature liquid water by capillary action from a pool beneath the sample. Water boils in the porous copper, with vapor escaping to the ambient atmosphere. Condensate is prevented from flooding the active region by a second cellulose wick positioned above.

Small-scale heat transfer experiments with high heat fluxes are generally challenging due to the influence of conductive heat spreading. We minimize this effect here by the use of glass substrates with relatively low thermal conductivity (~1 W m^{-1} K^{-1}) upon which the active region is formed and by the direct application of heat to the active region by volumetric electrical resistance heating. We have characterized the effects of parasitic conduction in the system, and found them to be small as discussed later and in the supplementary material.[20]

The porous active region is formed by electrodeposition of copper. We use randomly packed, monodisperse polystyrene spheres as a sacrificial template to pattern the pore spaces of the copper, as described previously.[21] Fig. 1(c), a

[a]Authors to whom correspondence should be addressed. Electronic addresses: Juan.Santiago@stanford.edu and James.Palko@stanford.edu

 © 2015 AIP Publishing LLC

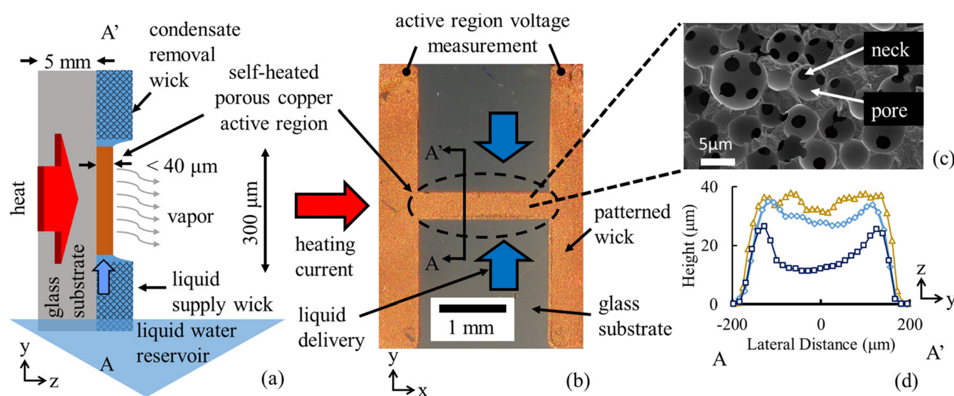

FIG. 1. Boiling experiment using volumetrically Joule heated porous copper structures with passive capillary feeding of water. (a) Schematic of heat transfer experiment cross section A-A′ showing liquid feed from stagnant pool and condensate removal. (b) Image of actual patterned porous copper layer sample, shown here without supply or condensate removal wicks. Labels indicate current delivery to and voltage measurement across active region. (c) Scanning electron micrograph of templated electrodeposited porous copper. (d) Length-averaged cross-sections of active regions for three porous copper samples used in heat transfer experiments.

scanning electron micrograph, shows the resulting structure following copper electrodeposition and template dissolution. The random packing of monodisperse spheres, expected to result from the drop casting process used to create the template, provides volume filling between 56% and ∼64%[22] with corresponding porosities of the inverse structures. Porous copper films with similar preparation show excellent thermal conductivity ($170\,\mathrm{W\,m^{-1}\,K^{-1}}$)[23] and permeability ($10^{-13}\,\mathrm{m^2}$).[21,24]

The shape of the working electrode driving electrodeposition defines the lateral dimensions of the porous layer. The amount of applied charge determines thickness. We use gold evaporation and a contact mask to pattern a thin (e.g., 50 nm) gold film working electrode in the desired shape of the porous copper region. As shown in Fig. 1(b), in addition to the narrow ($2\,\mathrm{mm} \times 0.3\,\mathrm{mm}$) active region, the porous copper layer forms large contact pads on either side of the heated area to allow supply of current to and measurement of voltage across the active region. These pads are large enough (∼13 times wider than the active region) to contribute negligibly to overall resistance and minimize heating outside the active region. Fig. 1(d) shows length-averaged active region cross-sections obtained by profilometry of three samples for which heat transfer measurements were performed.

The active regions provide electrical resistances of tens of milliohm (e.g., 20 mΩ) depending on the specific cross section. We used electrical resistance thermometry to determine active region temperature with a four-point measurement and using the active region itself as the resistive element. The measured temperature thus represents an average value based on the net electrical resistance of the active region. Before heat transfer characterization, we calibrated active region resistances of each sample under controlled, uniform temperature conditions (see supplementary material[20]) and found them to obey a highly linear relationship with a temperature coefficient of resistivity of $(3.857 \pm 0.002) \times 10^{-3}\,\mathrm{K^{-1}}$, similar to that reported for bulk Cu.[25] We note that copper has frequently been applied in resistance thermometry[26] displaying high accuracy.[27] Systematic errors for both active region temperature and power dissipation measurements during heat transfer experiments were estimated to be 1%.

Fig. 2 summarizes measurements of area power density dissipated in the porous copper layer for three separate samples (diamonds, triangles, and squares) versus active region temperature. More than $1200\,\mathrm{W\,cm^{-2}}$ (in addition to heat loss due to conduction) can be dissipated by boiling with passive capillary feed at a superheat of <10 K (∼110 °C bridge temperature) for the best performing sample. Superheat for all samples are <13 K at maximum dissipation. Fig. 2 shows data for operation of the active region with steady current supply. We exclude measurements taken during variation of heating current, defined as transients exceeding $5\,\mathrm{mA\,s^{-1}}$ and a 5 s settling period following the end of the transient. We determined parasitic heat losses not due to boiling using separate dry measurements for one porous copper sample (see supplementary material[20]). The latter experiment shows that parasitic heat losses account for $\sim 110\,\mathrm{W\,cm^{-2}}$ at maximum active region temperature (∼113 °C). The dry measurements correspond closely to the wet counterparts at temperatures below those where boiling occurs, indicating that conduction likely dominates heat dissipation for the wetted porous copper at

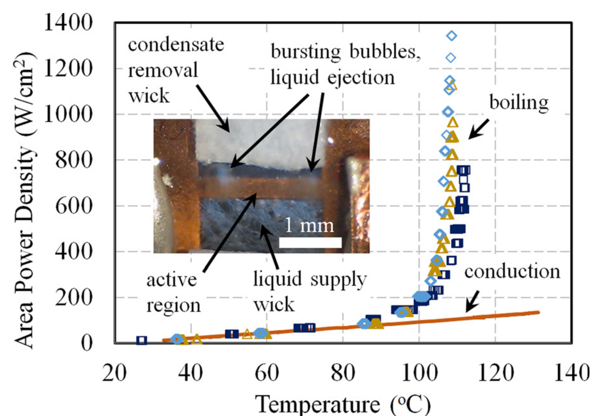

FIG. 2. Total measured area power density dissipation versus active region temperature for boiling of water from three electrodeposited porous copper samples (diamonds, triangles, and squares), and for conduction from a single porous sample without liquid feed (solid line). The inset shows a micrograph of the active region during boiling with total power dissipation of $560\,\mathrm{W/cm^2}$. Bubble formation, burst, and liquid ejection events are observed during boiling.

power densities below about 85 W cm^{-2}. We observe vigorous boiling at the active region corresponding to the dramatic increase in heat dissipation along with a distinct acoustic signature (data not shown) and violent ejection of liquid (Fig. 2 inset). These observations are consistent with experiments[7,28] and models[2,29] characterizing the formation and growth of vapor bubbles within the porous structure and their subsequent escape comprising the boiling process in porous media.

The maximum heat flux observed for the porous samples is consistent with a partial loss of cooling and, eventually, burnout due to the volumetric self-heating. Maximum heat fluxes corrected for parasitic losses, $q''_{corr\ max}$, show substantial variation between the samples measured (~60% of the mean). This variation is partially accounted for by the differences in thickness of the active regions of the three samples. Critical volume power density corrected for parasitic conduction and normalized by the mean active region thickness, $q'''_{corr\ max}$, shows a significantly smaller range (<30% of average) than critical heat flux for the samples considered (see supplementary material[20]). The remainder of variability in heat dissipation is likely due to differences in microstructure of the active region resulting from processing variability and the random nature of the structure. The thickness of the porous copper active region (<40 μm) is less than 8 times the characteristic microstructural feature size (5 μm). We therefore expect significant intrinsic local variability in both electrical and fluidic transport properties of the structure, resulting in variation of the heat density, which can be dissipated without local cooling failure.

Maximum supported heat flux in capillary fed systems is commonly determined by liquid supply limitations.[2] The short transport length of the active region here (nominally 150 μm due to recycling of the condensate at the top of the sample) alleviates this capillary transport limitation and allows dissipation of extremely high heat fluxes. We also note that some portion of the active region may be covered by a contiguous liquid film which could aid in liquid transport (though this is difficult to quantify). The maximum pressure drop due to flow through the porous bulk from the edge to centerline of the active region can be estimated as

$$\Delta p_{liq\,max} = -\frac{\mu}{2\kappa\kappa_{rl}}\frac{q'''_{corr\,max}}{h_{fg}\rho}L^2, \quad (1)$$

where μ is liquid dynamic viscosity, κ is intrinsic permeability of the porous copper, κ_{rl} is relative permeability for the liquid phase due to partial vapor saturation of the structure, h_{fg} is heat of vaporization, ρ is liquid density, and L is effective wicking length, set here to 150 μm. Here we have assumed spatially uniform vaporization throughout the structure. We can expect partial dryout when this pressure drop exceeds the capillary suction available from the porous structure as determined by the pore diameter.

For the mean critical volumetric power dissipation observed, $q'''_{corr\ max} = 346$ kW cm^{-3}, the measured permeability of the porous structure (10^{-13} m^2),[21,24] and properties of liquid water at 110 °C (surface tension, $\gamma = 57$ mN m^{-1}, $\mu = 0.255$ mPa s),[30] equating capillary suction and maximum viscous pressure drop gives mean relative liquid permeabilities of 0.1 for negligible water/copper contact angle or 0.3 for a higher contact angle (72°) as reported for the water/copper system at elevated temperature (101 °C).[31] We hypothesize that these reduced apparent liquid permeabilities may be the result of steady state vapor saturation of the structure and/or transient generation of bubbles in various pores during boiling.

After boiling is initiated, the system shows very low differential thermal resistance, dT/dq''_{corr}, where T is the measured active region temperature, and q''_{corr} is the corrected heat flux referenced to the active region base area. For example, the best performing sample shows a superheat of less than 10 K at maximum dissipation (>1200 W cm^{-2} in addition to conductive losses), with superheat varying less than 5 K over a range of input heat fluxes exceeding 1000 W cm^{-2}. We attribute the observed superheat behavior primarily to three effects strongly related to feature size of the structure: confinement of vapor bubbles, capillary suction in the liquid phase, and conduction through thin liquid films.

One mechanism likely to significantly influence superheat is the capillary pressure in nucleating vapor bubbles due to confinement within the porous structure.[2] Consider that the characteristic diameter of the spherical pores (5 μm) in the copper layer may correspond to a capillary pressure in a vapor bubble with a similar diameter in water at 110 °C of about 45.4 kPa. This elevation of the vapor pressure results in an effective superheat (an increase in saturation temperature) of 11 K, for a pressure in the surrounding liquid equal to ambient (101 kPa). In our experiments, we found that significant boiling occurs below this value for superheat (e.g., 5–6 K). We hypothesize that this discrepancy may be due to variability in the size of the template spheres and the reduction in curvature of the liquid vapor interface allowed by the necks connecting adjacent pores. In any case, the confinement effect of the porous structure should operate at all heat fluxes higher than that required for boiling, and should provide a relatively constant offset between vapor pressure in bubbles and pressure in the surrounding liquid.

Unlike the geometry-driven confinement contribution, the liquid pressure is condition dependent and non-uniform throughout the porous structure. Liquid pressure everywhere in the structure should be at or below ambient due to the viscous losses associated with flow through the wick. This reduction in liquid pressure should decrease the absolute pressure within vapor bubbles and consequently lower the saturation temperature, i.e., viscous losses should partially counteract the confinement effect of the porous structure and reduce the superheat associated with it. Global liquid flow rate and corresponding viscous pressure loss scales with dissipated heat flux. In the supplementary material,[20] we present a brief analysis of the estimated coupled, non-uniform effects of capillary suction, viscous losses, and bubble capillary pressures. This simple analysis suggests a dependence of mean vapor pressure inside bubbles, $\overline{p_{vap\,bub}}$, within the porous structure given by

$$\overline{p_{vap\,bub}} = p_{amb} - \frac{2}{3}\frac{\gamma}{r_{pore}}(3 - 2\cos\theta), \quad (2)$$

where p_{amb} is the ambient pressure, r_{pore} is the pore radius, and θ is the water/copper contact angle. The corresponding estimated reductions in confinement associated superheat are 2–7 K, depending on water/copper contact angle as previously discussed.

The coupled mechanisms discussed earlier affect the vapor pressure at evaporating surfaces and corresponding saturation temperature. The last mechanism we consider here is thermal resistance due to conduction from the surface of the self-heated copper structure to the evaporating surface. The temperature difference associated with this conduction also contributes to observed global superheat values. Conduction resistance in thin evaporating liquid films has been extensively analyzed and shown to be an important component of observed superheat, e.g., for individual menisci on heated surfaces[32] and boiling in porous layers.[29] We here present a brief order of magnitude estimate of this effect. We consider an effective liquid film thickness for the entire internal surface. This idealized film encompasses the effects of all transients and spatial variations of the liquid/vapor distribution. The observed thermal resistance (referenced to the active region base area) resulting from conduction through a planar film of effective thickness, d_{film}, is then

$$\frac{\Delta T}{\Delta q''_{corr}} = \frac{d_{film}}{k_{liq}} \frac{A_{base}}{A_{act}}, \tag{3}$$

where, k_{liq} is the thermal conductivity of water (0.68 W m^{-1} K^{-1} at 110 °C),[30] and A_{base} and A_{act} are the projected base area and active internal surface area of the structure, respectively. The radius of the pores (2.5 μm) in the structure provides a maximum upper bound for d_{film}. The observed differential thermal resistance of the structures at high heat fluxes (e.g., 0.003 K cm^2 W^{-1}) then suggests an area enhancement A_{act}/A_{base} less than 12 for an idealized film approximated as planar. This enhancement represents about 0.5 of the internal surface area available from a 35 μm thick porous layer with 60% porosity (potential area enhancement >25 times). Actual films in the structure during boiling must be substantially less than the 2.5 μm upper bound due to finite vapor saturation. This implies that the actual internal surface area participating in boiling may be significantly less than 0.5, with the remainder likely inactive due to heterogeneous and transient phase distribution.

Fig. 3 shows a comparison of the current work with a selection of published studies. We compare heat flux dissipation corrected for parasitic losses, q''_{corr}, versus temperature for our structure to data reported recently for capillary fed structures operating with water in boiling/evaporation.[7–10,12,14] Structures have been demonstrated which dissipate heat fluxes comparable with those reported here, but generally at significantly higher superheats.[8,10] There are a variety of reasons for this difference. The structures from literature shown in Fig. 3 all have significantly larger lateral extents than the current system, and these are heated from beneath (sometimes through a thermal interface material). In some cases,[9,10,12] the effect of conductive spreading may reduce the heat flux at the base of the porous structure below the (higher) reported value. Those structures exhibiting large superheat at high heat flux or significant changes in slope for heat flux versus temperature[8,10,11] likely suffer from partial dryout. The current system seems to avoid these effects, and this is likely a result of both our short transport length and the effects of porous structure discussed earlier. We note that structures with larger transport lengths generally also rely on larger feature sizes to increase permeability,[8,10,11,33] and this has significant effects on superheat. Conversely, fine featured (9 μm) structures have been microfabricated that show comparable superheats with the current structures at lower maximum heat flux.[12]

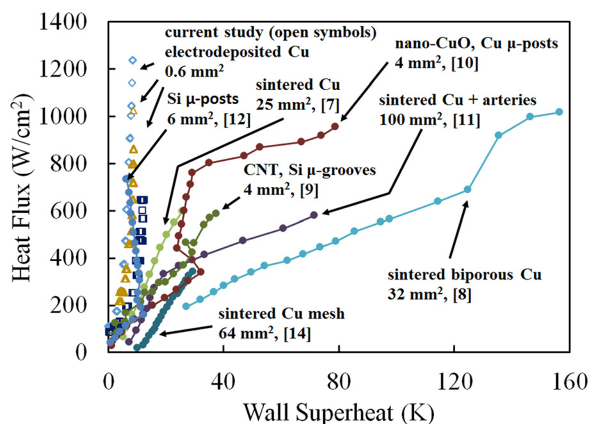

FIG. 3. Heat flux dissipation versus superheat for a variety of porous structures. The heat flux dissipation for the current study (open diamonds, triangles, and squares) is corrected for conduction losses. Other data (filled circles and lines) are from wicking structures with high heat flux from recent studies.[7–10,12,14] Wick construction and heated area are indicated for each system.

In conclusion, we here report a thin electrodeposited porous copper wick that demonstrates the ability to dissipate high heat fluxes (>1200 W cm^{-2}) with minimal (and heat-flux insensitive) superheat (<10 K at >1200 W cm^{-2}) using fine (5 μm) features. The superheat changes by <5 K over a heat flux range of >1000 W cm^{-2}. The data suggest that fine feature sizes facilitate the excellent superheat performance but incur a significant penalty in terms of permeability, and this limits the length scales over which these structures can operate. The performance demonstrated is most directly applicable to the cooling of hot spots with extreme heat fluxes such as those encountered in radio frequency amplification, laser diode, and microelectronic applications.[34] However, the extension of this heat transfer performance to larger areas and transport lengths will likely require the implementation of hierarchical liquid distribution schemes to circumvent the fluidic limitations of the fine featured structures. One attractive option may be three-dimensional manifolding.[35] Unlike two-dimensional schemes (such as transport "arteries"[11]), three-dimensional flow supplies have potential to avoid the sacrifice of heat dissipation area and/or exposure of inlet liquid channels to high heat fluxes. These cooling applications would generally entail heating from the substrate supporting the porous structure in contrast to the volumetric heating demonstrated here. However, the high thermal conductivity (170 W m^{-1} K^{-1}) of the porous copper and the minimal thermal contact resistance facilitated by the electrodeposition fabrication process allow effective application to substrate heated applications (e.g., with conduction across a 40 μm thick porous layer dissipating 1 kW cm^{-2} accounting for ~1 K temperature change).

This project was supported in part by the U.S. Defense Advanced Research Projects Agency Microsystems Technology Office ICECool Fundamentals Program under Award No. HR0011-13-2-0011. Disclaimer: The views,

opinions, and/or findings contained in this article are those of the authors and should not be interpreted as representing the official views or policies, either expressed or implied of the Defense Advanced Research Projects Agency or Department of Defense. Part of this work was performed at the Stanford Nano Shared Facilities (SNSF).

[1]J. R. Thome, *Enhanced Boiling Heat Transfer* (Taylor & Francis, 1990).
[2]A. Faghri, *Heat Pipe Science and Technology* (Taylor & Francis, Washington DC, 1995).
[3]J. A. Weibel and S. V. Garimella, Adv. Heat Transfer **45**, 209 (2013).
[4]V. K. Dhir, Annu. Rev. Heat Transfer **5**, 303 (1994).
[5]F. A. L. Dullien, *Porous Media: Fluid Transport and Pore Structure*, 2nd ed. (Academic Press, 1992).
[6]D. A. Reay, P. A. Kew, and R. J. McGlen, *Heat Pipes*, 6th ed. (Butterworth-Heinemann, Oxford, 2014), pp. 15–64.
[7]J. A. Weibel, S. V. Garimella, and M. T. North, Int. J. Heat Mass Transfer **53**, 4204 (2010).
[8]T. Semenic and I. Catton, Int. J. Heat Mass Transfer **52**, 5113 (2009).
[9]Q. Cai and Y.-C. Chen, J. Heat Transfer **134**, 021503 (2012).
[10]Y. Nam, S. Sharratt, G. Cha, and Y. S. Ju, J. Heat Transfer **133**, 101502 (2011).
[11]G. S. Hwang, E. Fleming, B. Carne, S. Sharratt, Y. Nam, P. Dussinger, Y. S. Ju, and M. Kaviany, Int. J. Heat Mass Transfer **54**, 2334 (2011).
[12]D. Ćoso, V. Srinivasan, M.-C. Lu, J.-Y. Chang, and A. Majumdar, J. Heat Transfer **134**, 101501 (2012).
[13]Y. Zhao and C. Chen, in *Proceedings of the 2006 ASME International Mechanical Engineering Congress and Exposition (IMECE 2006)*, pp. 177–181.
[14]C. Li and G. P. Peterson, J. Heat Transfer **128**, 1320 (2006).
[15]X. Dai, M. Famouri, A. I. Abdulagatov, R. Yang, Y. C. Lee, S. M. George, and C. Li, Appl. Phys. Lett. **103**, 151602 (2013).
[16]R. Xiao, S. C. Maroo, and E. N. Wang, Appl. Phys. Lett. **102**, 123103 (2013).
[17]P. V. Braun and P. Wiltzius, Nature **402**, 603 (1999).
[18]M. L. K. Hoa, M. Lu, and Y. Zhang, Adv. Colloid Interface Sci. **121**, 9 (2006).
[19]O. D. Velev and A. M. Lenhoff, Curr. Opin. Colloid Interface Sci. **5**, 56 (2000).
[20]See supplementary material at http://dx.doi.org/10.1063/1.4938202 for details of experimental procedures and data analysis.
[21]T. J. Dusseault, J. Gires, M. T. Barako, Y. Won, D. D. Agonafer, M. Asheghi, J. G. Santiago, and K. E. Goodson, in *2014 IEEE Intersociety Conference on Thermal and Thermomechanical Phenomena Electronic Systems (ITherm)* (2014), pp. 750–755.
[22]H. M. Jaeger and S. R. Nagel, Science **255**, 1523 (1992).
[23]M. T. Barako, J. M. Weisse, S. Roy, T. Kodama, T. J. Dusseault, M. Motoyama, M. Asheghi, F. B. Prinz, Z. Xiaolin, and K. E. Goodson, in *2014 IEEE Intersociety Conference on Thermal and Thermomechanical Phenomena Electronic Systems (ITherm)* (2014), pp. 736–743.
[24]C. Zhang, G. Rong, J. W. Palko, T. J. Dusseault, M. Asheghi, J. G. Santiago, and K. E. Goodson, in *ASME 2015 InterPACK Conference* (ASME, 2015), paper IPACK2015-48262.
[25]R. A. Matula, J. Phys. Chem. Ref. Data **8**, 1147 (1979).
[26]*Practical Temperature Measurement*, edited by P. R. N. Childs (Butterworth-Heinemann, Oxford, 2001), pp. 145–193.
[27]R. C. Langlands, J. Sci. Instrum. **41**, 478 (1964).
[28]J. A. Weibel and S. V. Garimella, Int. J. Heat Mass Transfer **55**, 3498 (2012).
[29]H. F. Smirnov, J. Porous Media **4**, 33 (2001).
[30]P. J. Mallard and W. G. Linstrom, *NIST Chemistry WebBook, NIST Standard Reference Database Number 69* (National Institute of Standards and Technology, Gaithersburg, MD, 2015).
[31]A. Boyes and A. Ponter, Chem. Ing. Tech. **45**, 1250 (1973).
[32]H. Wang, S. V. Garimella, and J. Y. Murthy, Int. J. Heat Mass Transfer **51**, 6317 (2008).
[33]Q. Cai and C.-L. Chen, J. Heat Transfer **132**, 052403 (2010).
[34]A. Bar-Cohen and P. Wang, J. Heat Transfer **134**, 051017 (2012).
[35]Y. Won, E. N. Wang, K. E. Goodson, and T. W. Kenny, Int. J. Therm. Sci. **50**, 325 (2011).

SUPPLEMENTARY INFORMATION FOR:

Approaching the limits of two-phase boiling heat transfer: high heat flux and low superheat

J.W. Palko,[1,a)] C. Zhang,[1] J. Wilbur,[1] T. Dusseault,[1] M. Asheghi,[1] K. Goodson,[1] and J.G. Santiago[1,a)]

[1]*Department of Mechanical Engineering, Stanford University, Stanford, California, 94305, USA*

a) Authors to whom correspondence should be addressed. Electronic mail: Juan.Santiago@stanford.edu, James.Palko@stanford.edu

This document contains supplementary information and figures further describing experiments and analyses of boiling heat transfer in our capillary fed porous copper structures.

S-1: Experimental setup

S-2: Resistance thermometry calibration

S-3: Parasitic heat loss

S-4: Volumetric power density calculation

S-5: Coupled capillary and viscous effects on superheat

Number of pages: 6

Number of figures: 3

Number of tables: 1

S-1: EXPERIMENTAL SETUP

Fig. A1 shows a schematic of the setup used for electrical measurement during heat transfer characterization. A current source supplies heating current to the active region. We quantify heating current from voltage measurement across a current sensing resistor. We also measure voltage across the active region. Dissipated power equals the product of the measured heating current and active region voltage. The quotient of active region voltage over heating current provides the active region resistance, which is used to determine temperature of the active region by resistance thermometry as discussed below and in the main paper.

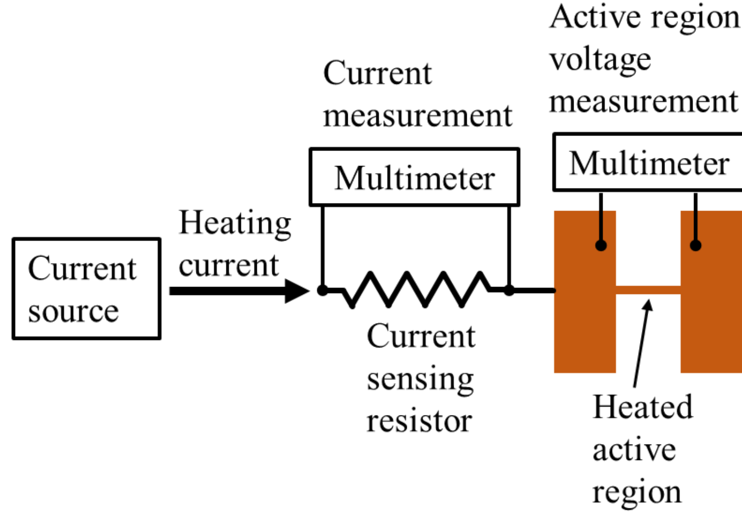

FIG. A1. Electrical measurement schematic for heat transfer characterization.

S-2: RESISTANCE THERMOMETRY CALIBRATION

Our calibration required measurement of active region electric resistance as a function of temperature. We characterized temperature dependence of the active region resistance of each sample used for boiling heat transfer experiments as well as an additional unused sample. We measured temperature dependence of the active region resistance inside an insulated chamber to achieve isothermal conditions. After sufficient equilibration time (typically a few minutes), a thermocouple pressed to the substrate, adjacent but not contacting the active region, measured substrate temperature. We controlled temperature in the chamber using an aluminum block with a large thermal mass compared to the remainder of the system and heated to a desired temperature. We sealed the chamber and allowed it to cool slowly, with temperature changes not exceeding 0.12 K min^{-1} after initial temperature homogenization. Fig. A2 shows the active region resistance, R_{ar}, normalized by the resistance value at 20 °C, R_{ar}(20 °C), versus substrate temperature for four samples along with a linear fit. The correlation is highly linear (R^2 = 0.9999), obeying the relation:

$$\frac{R_{ar}}{R_{ar}(20\,°\mathrm{C})} = 1 + \alpha(T - 20\,°\mathrm{C}) \tag{A1}$$

where α is the temperature coefficient of resistance for the active region, and has the value α = (3.857 $\pm$ 0.002) x 10^{-3} °C^{-1}, as determined by the linear fit with uncertainty defined by a 95% confidence interval.

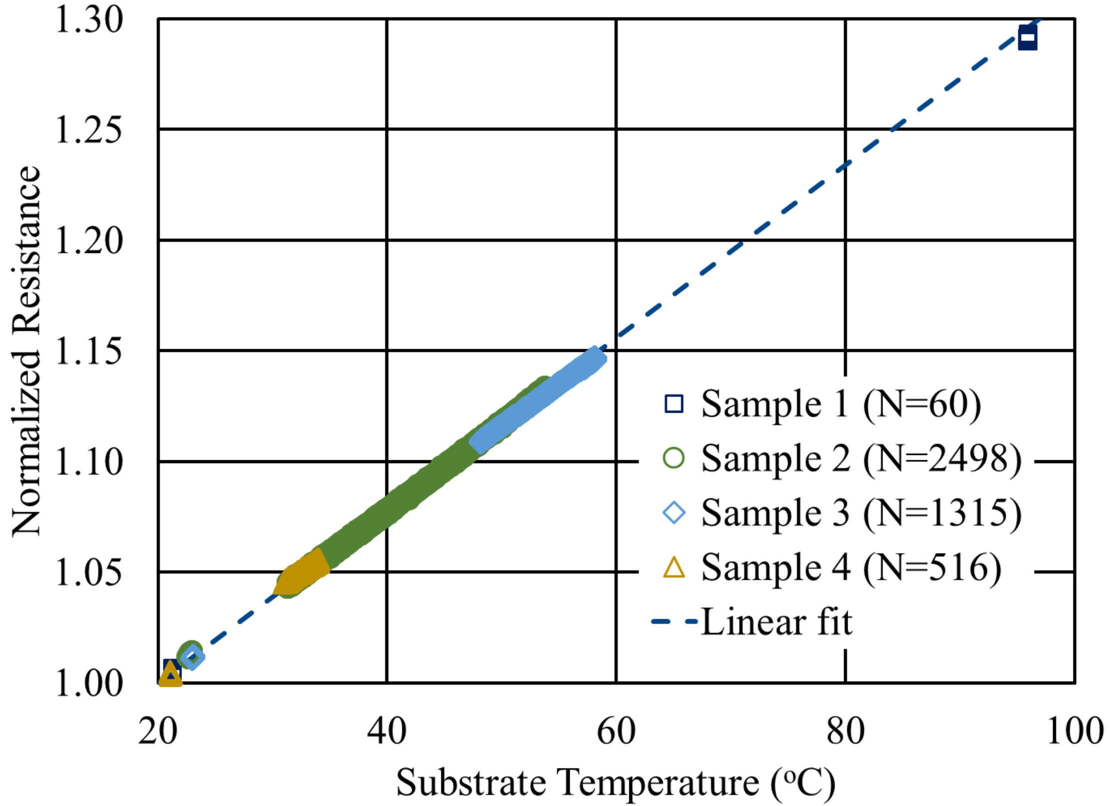

FIG. A2. Calibration of electrical resistance as a function of temperature for our porous metal structure. Plotted is active region resistance normalized by the resistance value at 20 °C versus substrate temperature for four porous copper samples, including the three samples used in boiling heat transfer experiments, and linear fit.

S-3: PARASITIC HEAT LOSS

In addition to the heat dissipated from the active region via boiling of the working fluid, heat also escapes due to several sources of parasitic loss including conduction into the substrate, radiation to the ambient, and free convection to the air. We characterized the contribution of these effects to the total heat dissipated from the active region as a function of temperature. We quantified parasitic loss as the power dissipated by the dry active region of a single porous copper sample with no liquid supplied to support boiling and with the active region held at fixed, elevated temperatures. The experimental setup for parasitic heat dissipation characterization was identical to that for boiling heat transfer characterization with the exception of the liquid supply and condensate removal wicks, which were omitted to prevent liquid supply to the active region, Fig. A3. The parasitic heat flux, q''_{para}, shows a linear trend with the difference in temperature between the active region, T, and ambient, T_{amb}, given by:

$$q''_{para} = (1.236 \pm 0.002 \text{ W cm}^{-2} \text{ K}^{-1})(\mathrm{T} - \mathrm{T}_{\mathrm{amb}}) \quad \text{(A2)}$$

.

with a regression coefficient of $R^2 = 0.999$, suggesting only minor effects due to radiation. We calculate corrected heat flux, q''_{corr}, accounting for heat dissipated in boiling as:

$$q"_{corr} = q"_{tot} - q"_{para}$$

, (A3)

where q''_{tot} is the total measured heat flux.

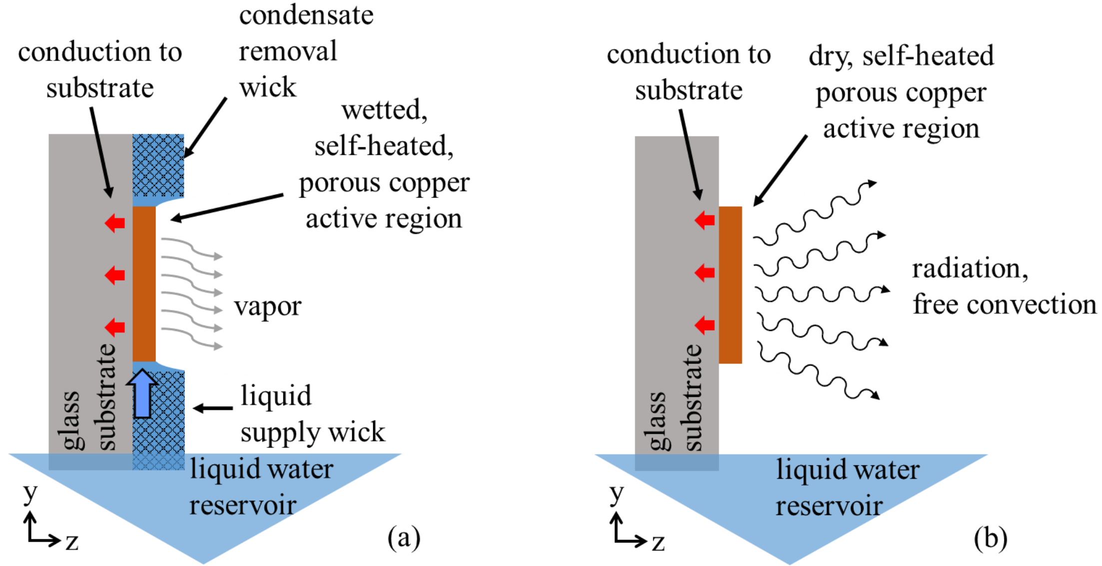

FIG. A3. Schematics of experimental setups for (a) two-phase, boiling heat transfer experiment and (b) a control experiment used to quantify parasitic loss due to conduction, radiative heat transfer, and simple free convection to the air.

S-4: VOLUMETRIC POWER DENSITY CALCULATION

We calculate corrected volumetric power dissipation due to boiling in the active region, q'''_{corr}, based on the corrected active region heat flux, q''_{corr}, (eq. A3) normalized by the mean thickness of the active region, t_{act}, as determined from profilometery (Fig. 1d.),

$$q'''_{corr} = \frac{q"_{corr}}{t_{act}}$$

(A4)

We define t_{act} as the length averaged cross sectional area (Fig. 1d.) divided by the width for each active region. Table A-I gives the maximum corrected area power dissipation, $q''_{corr\ max}$, and maximum corrected volumetric power dissipation, $q'''_{corr\ max}$, for the three samples measured.

TABLE A-I. Maximum active region power dissipation scaled by base area and volume and corrected for parasitic heat loss

Sample no.	$q''_{tot\ max}$ (W cm^{-2})	T @ $q''_{corr\ max}$ (^oC)	q''_{par} (W cm^{-2})	$q''_{corr\ max}$ (W cm^{-2})	t_{act} (μm)	$q'''_{corr\ max}$ (kW cm^{-3})
1	1340±13	109±1	105±1	1235	33.9	364±4
2	1130±11	110±1	106±1	1024	35.4	289±3
3	758±8	112±1	109±1	649	16.9	384±4
mean				969		346
range				586		95
range/mean				0.60		0.27

S-5: COUPLED CAPILLARY AND VISCOUS EFFECTS ON SUPERHEAT

Here we provide an analytical estimate of the effect of viscous pressure loss in reducing superheat due to capillary pressure in the confined pores of the porous copper structure. Apparent superheat due to increase in saturation temperature within a vapor bubble is given by:

$$\Delta T_{sat} = T_{sat}(p_{vap\ bub}) - T_{sat}(p_{amb}) \tag{A5}$$

where $p_{vap\ bub}$ and p_{amb} and are the pressures of the vapor in the bubble and the ambient atmosphere, respectively. Vapor pressure in the bubble is approximately related to the surrounding liquid pressure, p_{liq}, as follows:

$$p_{vap\ bub} = p_{liq} + \frac{2\gamma}{r_{bub}} \cong p_{liq} + \frac{2\gamma}{r_{pore}} \tag{A6}$$

where γ is liquid surface tension, r_{bub} is the radius of the vapor bubble, and r_{pore} is the pore radius. The current structure likely confines vapor bubbles to sizes close to those of the spherical pores themselves, providing a constant elevation in vapor pressure within the bubble of ~45 kPa for a 5 μm bubble in water at 110 ºC.

The pressure in the surrounding liquid, however, changes with heat flux and is non-uniform throughout the structure due to the viscous forces opposing flow. Assuming uniform heat dissipation throughout the active region volume, we approximate the pressure drop in the liquid from the edge of the structure ($x = 0$), where the liquid pressure equals ambient, to the center of the active region ($x = L$) as:

$$\Delta p_{liq}(x) = p_{liq}(x) - p_{amb} = \frac{\mu}{2\kappa\kappa_{rl}} \frac{q'''}{h_{fg}\rho} x(x - 2L) \tag{A7}$$

The mean liquid pressure drop is then given by:

$$\overline{\Delta p_{liq}} = \overline{p_{liq}} - p_{amb} = \frac{\int_0^{\mathrm{L}} \Delta p_{liq}(x)dx}{L} = \frac{\mu}{2\kappa\kappa_{rl}} \frac{q'''}{h_{fg}\rho} \frac{1}{L} \int_0^{\mathrm{L}} x(x-2L)dx$$

$$\overline{\Delta p_{liq}} = -\frac{2}{3} \frac{\mu}{2\kappa\kappa_{rl}} \frac{q'''}{h_{fg}\rho} L^2 = \frac{2}{3} \Delta p_{\max liq}$$

, (A8)

and equal to 2/3 of the maximum viscous pressure drop (eq. 1). At maximum heat dissipation (dryout) the maximum viscous pressure drop is expected to equal the capillary suction:

$$\Delta p_{\max liq} = \Delta p_{cap}$$

, (A9)

and capillary suction can be approximated as:

$$\Delta p_{cap} = -\frac{2\gamma \cos\theta}{r_{pore}}$$

, (A10)

where θ is the liquid/solid contact angle. Combining Eqs A6 and A8-10 yields an explicit expression for estimated average bubble vapor pressure at maximum heat flux as a function of ambient pressure, liquid surface tension, pore radius, and liquid/solid contact angle:

$$\overline{p_{vap\ bub}} = p_{amb} + \frac{2\gamma}{r_{pore}} - \frac{2}{3}\Delta p_{cap} = p_{amb} - \frac{2}{3}\frac{\gamma}{r_{pore}}(3 - 2\cos\theta)$$

. (A11)

The reduction in saturation pressure due to viscous pressure loss in the liquid corresponds to saturation temperatures that are lowered ~ 7 K for a negligible water/copper contact angle and ~ 2 K for a water/copper contact angle of 72°.